(Received 27 April 2026, Accepted 25 May 2026, Scheduled 13 June 2026)

Analysis and Evaluation of a Novel Linear Partitioned Primary Permanent Magnet Vernier Machine with Asymmetric Winding

Hui Feng and Meimei Xu*

School of Electrical and Information Engineering, Jiangsu University, Zhenjiang 212013, China

ABSTRACT: This paper proposes a high-thrust-density linear partitioned primary permanent magnet vernier (LPPPMV) machine based on an asymmetric winding configuration, leveraging the advantages of linear machines to avoid the unbalanced magnetic pull caused by asymmetric slot-pole combinations in rotary machines. Firstly, the winding factor and harmonic distribution of asymmetric slot-pole combinations are revealed from the perspective of armature MMF. Furthermore, a higher modulation ratio design is achieved under the same electromagnetic load, and its mechanism is analyzed. Then, to address the insufficient fault tolerance of conventional symmetric winding, a modular asymmetric winding machine is proposed and optimized. Consequently, the results show that the proposed machine exhibits superior characteristics in both thrust density and fault tolerance, and finally, experiments on a linear machine test bench validate the theoretical analysis.

1. INTRODUCTION

Due to the advantages of linear machines in cost and manufacturing, it is often used in linear motion processes, such as direct drive, railways, and industrial processing [1–3]. By eliminating complex transmission mechanisms and relying solely on magnetic coupling for energy transfer, linear machines offer advantages such as simple structure, high reliability, and efficient energy transmission. However, in conventional linear machines, armature winding and permanent magnets (PMs) are located in two separate parts of the machine [4–6]. This results in a significant amount of PMs usage being required for long-stroke applications, leading to high costs. To further improve the thrust density of the linear machine, the air-gap magnetic field modulation theory has been proposed [7]. The linear PM vernier (LPMV) machine has been studied based on the air-gap magnetic field modulation theory, aiming to reduce PM usage and further improve thrust density [8–11]. In this design, both the armature winding and PMs are located on the short primary, while the long secondary consists only of an iron core. Through the modulation effect, the stationary armature winding and PMs couple to transfer energy, enabling the machine to generate thrust force. However, the conventional LPMV machine faces the issue of insufficient thrust density. A linear partitioned primary permanent magnet vernier (LPPPMV) machine has been proposed to address this limitation [12–15]. In LPPPMV machines, the armature windings and PMs are located in the same primary part. Compared with the conventional linear machine, the armature windings and PMs in the LPPPMV machine are relatively fixed. The segmented primary allows the winding and PMs to be located in different parts. Through its segmented primary design, the new machine enhances the amplitude of specific orders of the permeance, thereby improving the thrust density of the machine.

The performance of vernier machines is closely related to the harmonic order of air-gap magnetic flux density. Novel magnetic-inductance theories for analyzing harmonics of air-gap magnetic flux density [16]. Besides, the number of slots and the pole count of the armature winding also affect harmonic order [17–19]. Adjusting the pole pairs of the armature winding requires identifying a specific armature winding arrangement. However, conventional slot-pole combinations are limited in number and cannot be adapted to more specific harmonics, thus failing to fully exploit the potential thrust density of the machine. Some studies have employed unconventional slot-pole combinations to weaken or enhance specific order harmonics, and though this affects various machine performance characteristics [20–22]. Since specific harmonics significantly influence the performance of the vernier machine, unconventional winding configurations can be utilized to manipulate these harmonics, thereby enhancing overall machine performance. Both primary segmentation and asymmetric winding can influence specific harmonics, but their combined effects have not yet been studied. Therefore, it is necessary to investigate the impact of applying asymmetric winding on the performance of the LPPPMV machines.

Besides, asymmetric slot-pole combinations offer advantages such as improved winding factor and reduced ripple, but they can cause adverse effects, such as unbalanced magnetic pull in rotary machines. By contrast, linear machines can fully leverage the benefits of asymmetric slot-pole configurations.

In this paper, the LPPPMV machines with symmetric and asymmetric winding configurations are compared. The mechanism underlying the improved modulation effect is analyzed from a perspective of harmonics. This paper is organized into

* Corresponding author: Meimei Xu (xmm0508@ujs.edu.cn).

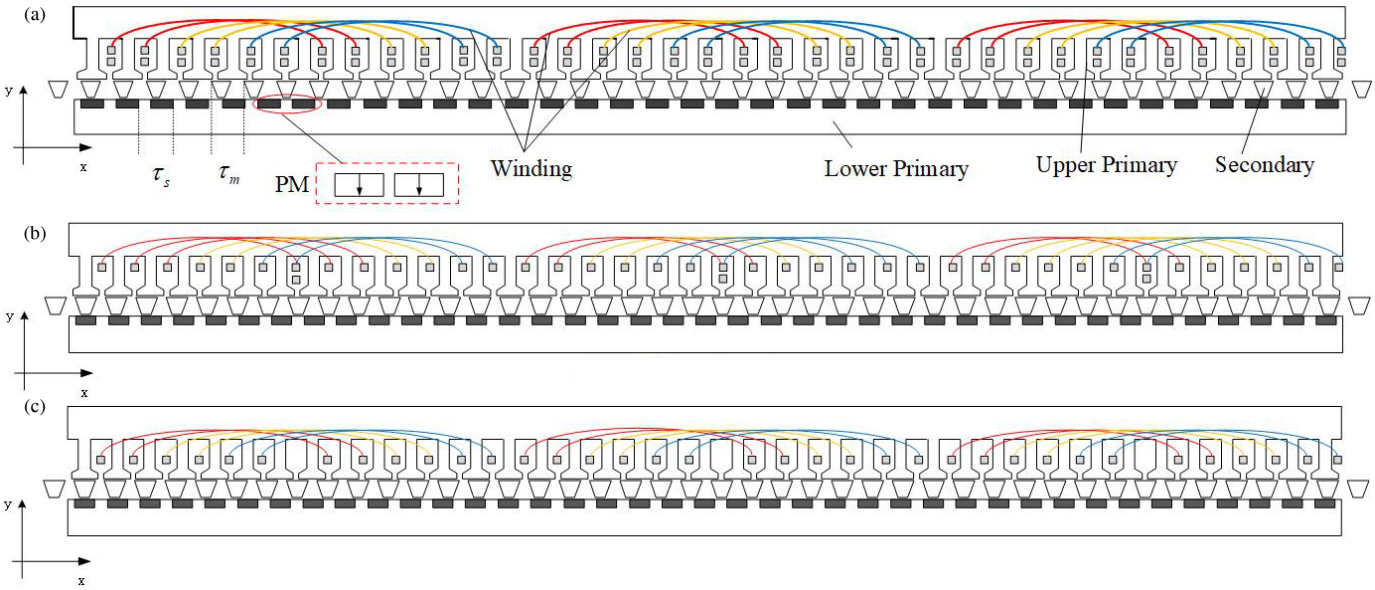

FIGURE 1. Winding configurations of the LPPPMV machine. (a) 36-slot. (b) 39-slot with $\tau = 7$. (c) 39-slot with $\tau = 6$.

five sections. Section 1 reviews the literature in related fields and introduces the research subject of this study. In Section 2, the topologies and winding connection methods of symmetric winding and asymmetric winding configurations are presented. In addition, the winding factor and harmonic distribution of asymmetric winding are analyzed from the perspective of armature winding magnetomotive force (MMF). From the perspective of magnetic field modulation theory, the operating mechanism of the asymmetric winding configuration is analyzed, and the performances of symmetric and asymmetric winding configurations are compared. In Section 3, a modular asymmetric LPPPMV machine is proposed and optimized, and the fault-tolerant performance of the modular LPPPMV machine is analyzed. In Section 4, the operating mechanism of the LPPPMV machine is analyzed from the perspective of magnetic field modulation theory, and how the asymmetric winding enhances the modulation ratio and back electromotive force (EMF) is investigated. Furthermore, a comparison of the back EMF and thrust force between the LPPPMV machine with conventional and unbalanced winding is provided. In Section 5, a prototype machine is built and tested to validate the effectiveness of the theoretical analysis. Finally, the conclusions are presented in Section 6.

2. TOPOLOGY AND WINDING ANALYSIS

2.1. Machine Topology

The conventional LPPPMV machine structure is shown in Fig. 1(a). From the perspective of the primary part, the primary of the LPPPMV machine is partitioned into two sections, with one section having 36 armature teeth and employing integral slot distributed winding, while the other houses vertically magnetized PMs. The secondary part has 39 iron cores in the middle that serve as modulation teeth. The conventional integral slot distributed winding design results in a modulation ratio of only 13, hindering the modulation effect and further improvement of thrust density. The proposed 39-slot asymmetric winding LPPPMV machine is depicted in Fig. 1(b) and Fig. 1(c). The total number of armature teeth and PMs has been changed to 39. The magnetization directions of the PM arrays are kept the same to ensure that their magnetic loading is identical. The number of turns in the armature windings is reduced, while the length of the PMs has been reduced to maintain consistency in electromagnetic load. Considering the fundamental pole pair number of the armature winding, the proposed 39-slot asymmetric winding employs mixed pole pitches, which are 6 and 7, respectively. The novel mixed pole pitches design and enhancement of a high modulation ratio result in higher no-load back EMF.

To satisfy the modulation theory, the relationship among the number of PM arrays P_{PM}, the number of effective modulating teeth P_s, and the number of pole pairs of the armature winding P_a is given as follows:

$$P_a = |P_s - P_{PM}| \tag{1}$$

To ensure a stable and continuous thrust force, the speed of the primary magnetic field, which is generated by PMs, must match that of the armature magnetic field. Furthermore, the number of pole pairs in the PM must correspond to that of the modulated armature magnetic field. Accordingly, the speed of the effective working flux can be derived as follows:

$$\nu_{PM} = \frac{P_s}{P_a}\nu \tag{2}$$

$$G_r = \frac{P_s}{P_a} \tag{3}$$

where G, v, and v_{PM} represent the modulation ratio, the speed of modulating teeth, and the speed of the air-gap magnetic field, respectively.

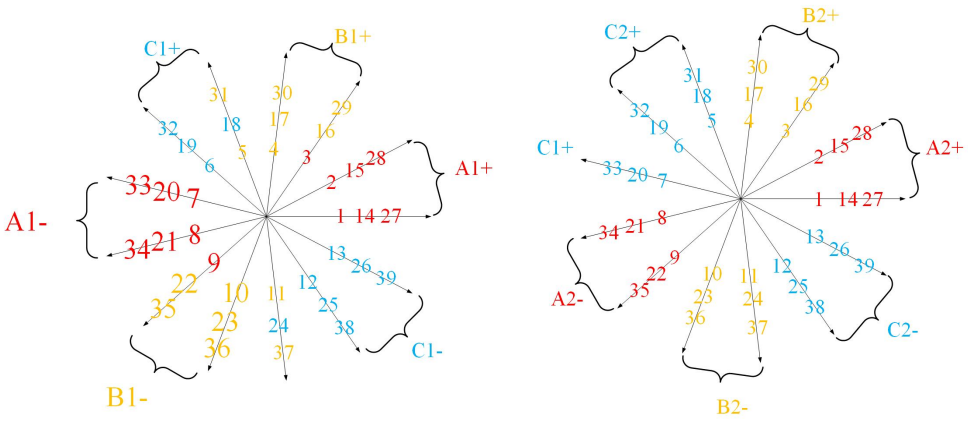

FIGURE 2. The diagram of the 39-slot asymmetric winding.

The two machines have the same number of armature winding pole pairs, P_a, and the winding connections are shown in Fig. 1(b) and Fig. 1(c). The 36-slot design adopts one pole pitch, which equals 6. The 39-slot design adopts two pole pitches, which are 6 and 7, respectively. The 36-slot phase-angle difference between phase windings is 120°, and the 36-slot design is as close to 120° as possible by using asymmetric winding.

Some design parameters are denoted in Fig. 1(a), and detailed parameters are shown in Table 1. It is worth noting that to ensure the fairness of the comparison, the width of the PM and the number of winding turns are adjusted to maintain equal electromagnetic loading. Additionally, the two motors used the same materials.

TABLE 1. Detailed parameters of two winding configurations.

Items	36-slot	39-slot
Primary pole pitch (mm)	17.5	16.2
Secondary pole pitch τ_m (mm)	16.2	15
Axial lamination length $L1$ (mm)	120	
Primary length L (mm)	630	
Primary slot opening bs0 (mm)	3	
Number of effective modulating teeth P_s	39	42
Number of PM arrays P_{PM}	36	39
Number of pole pairs of the armature windings P_a	3	
Speed of the primary v (m/s)	1.5	
Numbers of armature winding turns Na	43	40
Modulation ratio	13	14
PM width b (mm)	10.8	10
PM thickness a (mm)	5	
Rated current I (A)	1	
Overall airgap length (mm)	2	

2.2. Analysis of Asymmetric Winding Configuration

To improve the thrust performance of the LPPPMV machine, an asymmetric 39-slot winding configuration is adopted. The asymmetric 39-slot winding configuration can generate harmonics of different orders, and the back-EMF produced by some of these harmonics can contribute to improved performance. This section will provide a detailed analysis of some features of the winding.

The diagram of the asymmetric winding is shown in Fig. 2. As can be seen from Fig. 2, the 39-slot winding is composed of windings with pole pitches of 6 and 7. The windings with a pole pitch of 6 are labeled as A1, B1, and C1 in the diagram, while those with a pole pitch of 7 are labeled as A2, B2, and C2. It is worth noting that although they are designated as A1A2 here, there is no electrical isolation, and the same standard inverter is used. In the 39-slot design, windings with a pole pitch of 6 cannot be used to fill all the slots, while windings with a pole pitch of 7 would require more than 39 slots. Therefore, some of the windings with a pole pitch of 7 overlap with those having a pole pitch of 6. To analyze the characteristics of asymmetric winding, the MMF distribution and comparison of MMF orders are shown in Fig. 3 and Fig. 4, respectively. Compared with the symmetric 36-slot winding, the asymmetric 39-slot winding has the same third-order harmonic in its MMF, with a larger amplitude. It is worth noting that the fundamental MMF amplitudes differ because this comparison uses the same number of winding turns. When the number of winding turns is adjusted to ensure the same electric loading of the machines, the fundamental MMF amplitudes will become identical. It can be observed from Fig. 3(b) that, after adjusting the number of winding turns to maintain the same electric loading, the amplitudes of the third harmonic in the MMF of the two windings become nearly identical. Therefore, the subsequent improvement in performance originates from the increase in the product of the modulation ratio and the winding factor, rather than from the difference in the third harmonic. The purpose of this paper is not to compare the amplitudes of the fundamental MMF but to emphasize that the 39-slot configuration can still generate the third harmonic while maintaining a relatively high winding factor, thereby offering favorable conditions for adjusting the PM to enhance thrust. Furthermore, this configuration alters the order of the PM MMF harmonics, which positively influences thrust improvement.

In addition, the winding factor k_{wn} also needs to be analyzed. For more complex windings, the calculation of the winding factor requires analysis using the vector decomposition method.

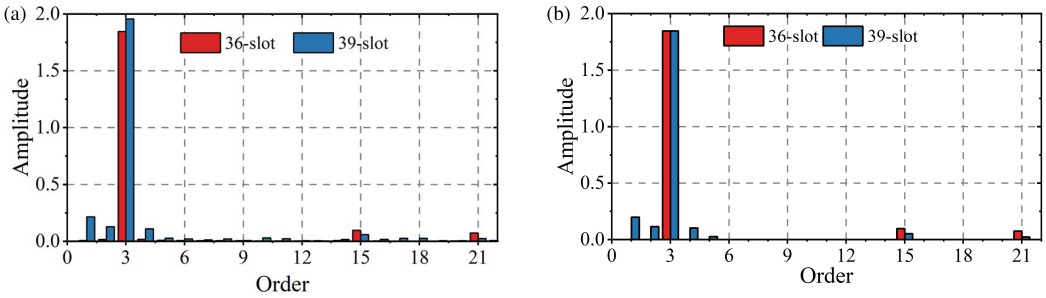

FIGURE 3. Comparison of MMF harmonics of both winding configurations, (a) with the same turns, (b) adjust the turns to keep the same electric load.

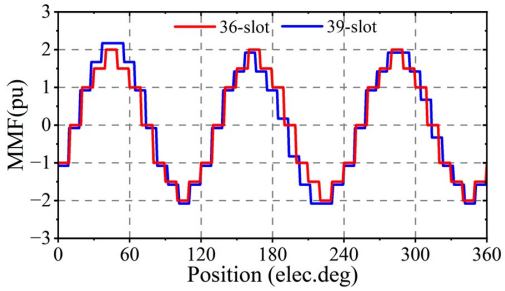

FIGURE 4. Total MMF distributions of both winding configurations.

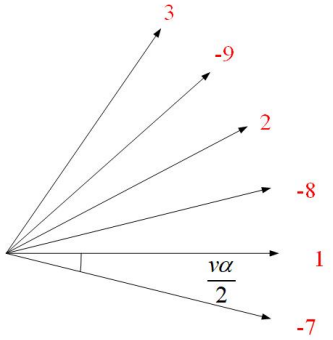

FIGURE 5. The conductor vectors belonging to phase A.

All the conductor vectors belonging to phase A are depicted in Fig. 5. Taking vector -8 as the reference vector, vector 1 can be expressed as:

$$\cos\left(\frac{v\alpha}{2}\right)+j\sin\left(\frac{v\alpha}{2}\right) \tag{4}$$

where α is the slot pitch angle.

Similarly, the expressions for the remaining vectors can be obtained from Table 2.

The final resultant vector can be decomposed into real and imaginary parts, expressed respectively as:

$$\begin{cases} \mathrm{Re}=\cos\left(3\dfrac{\nu\alpha}{2}\right)+7\cos\left(2\dfrac{\nu\alpha}{2}\right)+12\cos\left(\dfrac{\nu\alpha}{2}\right)+6 \\ \mathrm{Im}=-\sin\left(3\dfrac{\nu\alpha}{2}\right)-\sin\left(2\dfrac{\nu\alpha}{2}\right) \end{cases} \tag{5}$$

TABLE 2. The expression for a vector belonging to phase A.

vector	number	expression
(-7)	3	$\cos\left(2\frac{v\alpha}{2}\right)+j\sin\left(2\frac{v\alpha}{2}\right)$
(1)	6	$\cos\left(\frac{v\alpha}{2}\right)+j\sin\left(\frac{v\alpha}{2}\right)$
(-8)	6	1
(2)	6	$\cos\left(\frac{v\alpha}{2}\right)-j\sin\left(\frac{v\alpha}{2}\right)$
(-9)	4	$\cos\left(2\frac{v\alpha}{2}\right)-j\sin\left(2\frac{v\alpha}{2}\right)$
(3)	1	$\cos\left(3\frac{v\alpha}{2}\right)-j\sin\left(3\frac{v\alpha}{2}\right)$

The winding factor for the n-th harmonic is expressed as:

$$k_{wn}=\frac{\sqrt{\mathrm{Re}^2+\mathrm{Im}^2}}{N} \tag{6}$$

The finally calculated fundamental winding factor is given in Table 3. The winding factor for the 39-slot configuration is lower than that of its 36-slot counterpart. Due to the increased number of slots, the change in the order of the MMF harmonics also leads to a change in the back EMF.

TABLE 3. Comparison of winding factor between the two winding configurations.

k_{wn}	A phase	B phase	C phase
36-slot	0.966	0.966	0.966
39-slot	0.947	0.944	0.947

The 3rd-order no-load air-gap flux densities of these two machines are similar, which indicates that it is reasonable to improve the back EMF and thrust force through G_r and k_{wn}. Table 4 presents the product of G_r and k_{wn}, which reflects the magnitude of the modulation effect. This indicates an enhanced modulation effect with an increasing product of G_r and k_{wn}.

3. OPERATION PRINCIPLE

3.1. Air-Gap Flux Density and Back EFM

To analyze the influence of asymmetric winding on the LPPPMV machine's performance, the air-gap flux density

TABLE 4. The product of G_r and k_{wn}.

$G_r * k_{wn}$	A phase	B phase	C phase
36-slot	12.558	12.558	12.558
39-slot	13.258	13.216	13.258

is analyzed by means of the equivalent magnetic circuit method. The models of MMF and permeance are established. Key analytical expressions for the critical electromagnetic performance of the LPPPMV are derived, and their distinctive characteristics are investigated. To analyze the principle of magnetic field modulation more clearly and conveniently, the following assumptions need to be made: 1) The magnetic permeabilities of the primary and secondary parts are infinite, and the purpose is to neglect the magnetic saturation of the core. 2) The permeability of PM is equal to zero. 3) Neglect the end effects in the stacking direction of the linear machine lamination. 3) The magnetic field in the air gap varies only in the direction of motion (x-axis direction) and remains uniform in the normal direction (y-axis direction). 4) The MMF of PM is assumed as a square wave. Otherwise, the armature teeth and PMs of the primary teeth are salient, but this saliency should be considered in the MMF model. The modulation teeth should be considered in the permeance model.

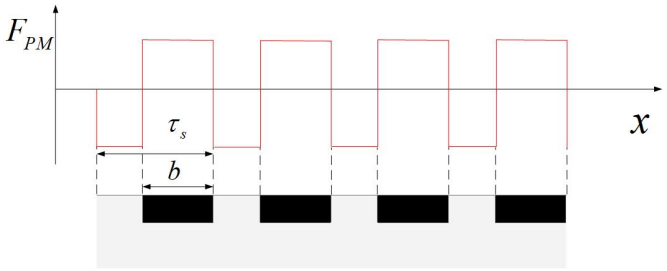

FIGURE 6. PM MMF of LPPPMV machine.

The PM MMF waveform in the LPPPMV machine is depicted in Fig. 6. Considering the consequent-pole PM array structure, the iron core between two adjacent magnetic poles can be considered to have opposite polarities. The magnitude of this polarity is related to the length of the iron core between the two PMs. The Fourier expression of the PM MMF of the LPPPMV machine can be expressed as follows:

$$F(x) = \sum_{i-1,3,5,\ldots}^{\infty} F_i \sin\left(2\pi i \frac{P_{pm}}{L} x\right) \tag{7}$$

$$F_i = \frac{2F_{pm}}{\pi i} \sin\left(\pi i P_{PM} \frac{a}{L}\right) \sum_{k=1}^{\infty} (-1)^{k+1} \cos[\pi i P_{pm} (2k-1) \frac{a}{L}] \tag{8}$$

where a represents the width of PM, P_{pm} the effective number of pole pairs of the PM in the direction of machine motion, and F_i the amplitude of each order of MMF harmonics after Fourier decomposition. Because of the consequent-pole PM arrays, one salient tooth and one PM can be regarded as a period. Therefore, 36 PM arrays have 36 periods. Due to its special structure, the LPPPMV machine with asymmetric winding enables an increase in the number of PMs without changing the pole pair number of the armature winding, thus enhancing the modulation ratio G_r of the LPPPMV machine.

Figure 7 compares the PM MMF distributions between the conventional and asymmetric winding configurations. As clearly shown in the figure under the same electromagnetic load, the MMF distribution of the PMs is modified from $36n$ to $39n$, where n is positive integer.

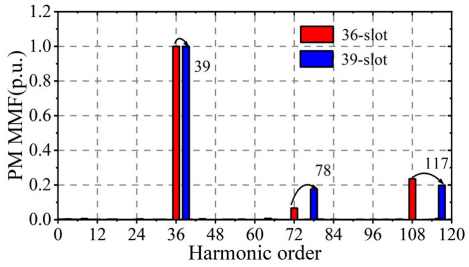

FIGURE 7. Comparison of PM MMF harmonics between the two winding configurations.

Because conventional and asymmetric winding LPPPMV machines have the same modulating teeth, depicted in Fig. 8, their permeance models are the same and can be expressed as follows:

$$\Lambda(x,t) = \Lambda_0 + \sum_{j=1,3,5,\ldots}^{\infty} \Lambda_j \cos\left[j \frac{2\pi}{L} \cdot P_s(x - \nu_s t)\right] \tag{9}$$

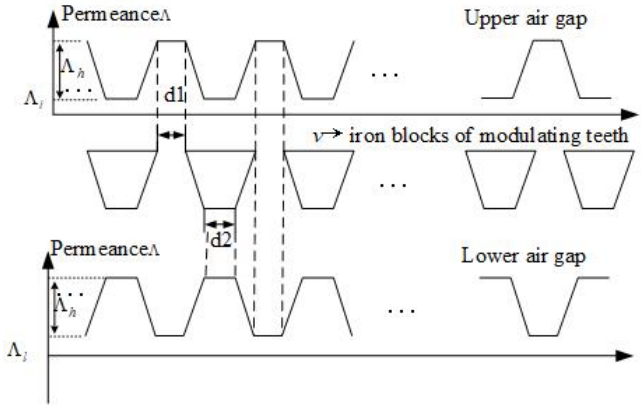

FIGURE 8. Permeance model of the LPPPMV machine.

The permeance of the upper air gap can be expressed as:

$$\begin{cases} \Lambda_0 = \dfrac{P_s}{L}(d_1\Lambda_h + d_2\Lambda_l) \\ \Lambda_j = \dfrac{2}{j\pi}(\Lambda_h - \Lambda_l)\sin(jd_1P_s\dfrac{\pi}{L}) \end{cases} \tag{10}$$

In the lower air gap, the permeance can be expressed as:

$$\begin{cases} \Lambda_0 = \dfrac{P_s}{L}(d_2\Lambda_h + d_1\Lambda_l) \\ \Lambda_j = \dfrac{2}{j\pi}(\Lambda_h - \Lambda_l)\sin(jd_2P_s\dfrac{\pi}{L}) \end{cases} \tag{11}$$

where d_1 and d_2 represent the upper width and lower width of the trapezoidal modulation teeth, respectively.

It should be noted that although the permeance distributions of the upper and lower air gaps are different, their influence on the back EMF depends on the direction of the flux density harmonics. Finite element analysis shows that the dominant 3rd and 36th harmonics have the same direction in both the upper and lower air gaps. Therefore, the contributions of the upper and lower air gaps are linearly superimposed and can be combined into an equivalent airgap flux density, eliminating the need to distinguish them separately in the analytical derivation. This conclusion is validated by finite element method (FEM).

The air-gap flux density can be calculated by multiplying the PM MMF and the air-gap permeance. Therefore, the no-load air-gap flux density of the LPPPMV machine can be expressed as follows:

$$\begin{aligned} B(x,t) &= F(x)\lambda(x,t) \\ &= \Lambda_0\sum_{i=1}^{\infty}F_i\cos\left(iP_{pm}\frac{2\pi}{L}x\right) \\ &\quad+\sum_{i=1}^{\infty}\sum_{j=1}^{\infty}F_i\Lambda_j\frac{\cos\alpha+\cos\beta}{2} \end{aligned} \tag{12}$$

$$\begin{cases} \alpha = (iP_{pm}+jP_s)\dfrac{2\pi}{L}x - jP_s\dfrac{2\pi}{L}(x+\nu_s t) \\ \beta = (iP_{pm}-jP_s)\dfrac{2\pi}{L}x + jP_s\dfrac{2\pi}{L}(x+\nu_s t) \end{cases} \tag{13}$$

The winding function method will be used to derive the expression for the back EFM of the LPPPMV machine. Since the end effects only influence the thrust ripple but do not affect the average thrust, the end effects of the machine are neglected to simplify the calculation, and the winding function of the armature winding can be expressed as:

$$\begin{cases} N_{\mathbf{A}}(x) = \displaystyle\sum_{n=1,3,5,\ldots}^{\infty} N_n\cos\left[n\frac{2\pi}{L}P_{\mathbf{a}}x\right] \\ N_{\mathbf{B}}(x) = \displaystyle\sum_{n=1,3,5,\ldots}^{\infty} N_n\cos\left[n\frac{2\pi}{L}P_{\mathbf{a}}\left(x-\frac{L}{3P_{\mathbf{a}}}\right)\right] \\ N_{\mathbf{C}}(x) = \displaystyle\sum_{n=1,3,5,\ldots}^{\infty} N_n\cos\left[n\frac{2\pi}{L}P_{\mathbf{a}}\left(x+\frac{L}{3P_{\mathbf{a}}}\right)\right] \end{cases} \tag{14}$$

$$N_n = \frac{2N_sk_{wn}}{n\pi P_a} \tag{15}$$

where N_A is the winding function of phase A, N_n the amplitude of each harmonic order of the winding function, N_s the number of series turns per phase, and k_{wn} the winding factor of the n-th harmonic.

According to electromagnetic field theory, the flux linkage per phase of the LPPPMV machine can be derived from the integral of the no-load air-gap flux density and the winding function. Taking phase A as an example, its expression is as follows:

$$\psi_A = L_{stk}\int_0^L B(x,t)N_A(x)dx \tag{16}$$

where L_{stk} is the effective length of the machine core lamination in the stacking direction.

According to Faraday's law of electromagnetic induction, taking phase A as an example, the no-load back EFM of the LPPPMV machines can be expressed as:

$$\begin{aligned} e_{\mathrm{A}}(t) &= -\frac{\partial\psi_{\mathrm{A}}(t)}{\partial t} \\ &= L_{xk}F_i\sum_{i-1,3,5,\ldots,j-1,3,5,\ldots}^{\infty} \\ &\quad\Lambda_j\frac{N_sk_{\mathrm{wn}}}{nP_{\mathrm{a}}}iP_s\nu_s\cos(\frac{2\pi}{L}P_s\nu_st) \end{aligned} \tag{17}$$

From the equation above, it can be observed that the back EMF of the LPPPMV machine is proportional to two parameters, namely G_r and k_{wn}. As analyzed in the previous section, the two parameters G_r and k_{wn} for conventional and asymmetric winding are compared. Table 4 shows that the asymmetric winding enhances the product of these two parameters, thus effectively improving the performance of the unconventional LPPPMV machine.

Other parameters, such as the fundamental air-gap flux density and thrust per ampere, are affected by nonlinear factors (saturation, leakage, temperature) and thus vary with operating conditions. In contrast, the product $G_{r*}k_{wn}$ is determined solely by machine topology and winding geometry, making it a load-independent design variable. Therefore, it serves as a reliable control variable for a fair comparison. The validity of this choice is confirmed by the close agreement between the predicted improvement (6.9%) and the FEM/experimental results ($\approx$ 6.7% and 6.4%, respectively).

3.2. Performance Analysis

Figure 9 depicts the A-phase no-load back EFM of two winding configuration machines. Compared with the 36-slot configuration, the no-load back EFM amplitude of the 39-slot configuration increases from 299.1 V to 319.2 V, representing an improvement of approximately 6.7%. In addition, the no-load back EMFs of both machines exhibit a highly sinusoidal waveform, with the total harmonic distortion (THD) values of 1.9% and 0.6%, respectively.

The improvement in no-load back EMF has also led to an increase in thrust force. The thrust force waveforms under the

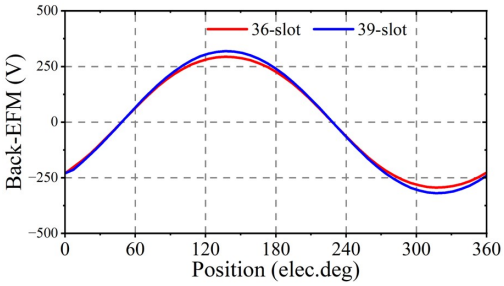

FIGURE 9. A-phase no-load back-EFM between the two winding configurations.

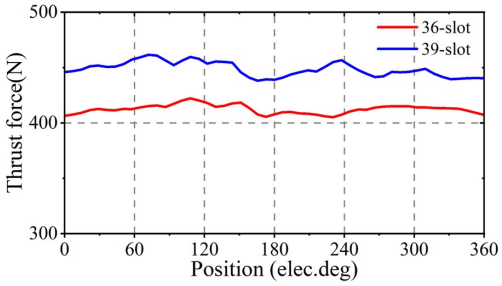

FIGURE 10. Thrust force performance between the two winding configurations.

rated current of 1 A and rated speed of 1 m/s are compared in Fig. 10. It can be observed that, because of the improvements in the winding configuration, the modulation effect has been enforced, and the average thrust of the machines has increased from 412 N to 442 N, while the thrust ripple has changed from 4.33% to 6.03%.

As shown in Table 1, the conventional and asymmetric winding LPPPMV machines share the same electromagnetic load. However, the asymmetric winding achieves a higher $G_r{*}k_{wn}$ value, indicating a stronger magnetic gear effect and a higher back EMF. Therefore, it can be concluded from the above analysis that the asymmetric winding effectively enhances the performance of the LPPPMV machine.

As shown in Table 5, at the rated current of 1 A, the 39-slot machine exhibits a slightly lower copper loss (5.94 W vs. 6.45 W) and a higher efficiency (84.1% vs. 82.3%) than the 36-slot machine. It is confirmed that the asymmetric winding maintains its superiority even when loss differences are considered.

TABLE 5. Performance comparison including copper loss and efficiency.

	resistance	copper loss	efficiency
36-slot	2.15	6.45	82.3
39-slot	1.98	5.94	84.1

4. FAULT TOLERANT WINDING CONFIGURATION

4.1. Fault-Tolerant Analysis with Modular LPPPMV Machine

Although the proposed LPPPMV machine with asymmetric winding configuration exhibits significant improvement in thrust force compared with its symmetric-winding counterpart, its fault-tolerant capability needs to be enhanced. For this machine, an open-circuit or short-circuit fault in the winding exacerbates the three-phase balance, resulting in significant thrust ripple and reduced average thrust force, which ultimately prevents normal operation. Moreover, the asymmetric winding configuration results in interphase winding overlap and an excessive coil span, thereby rendering the machine more susceptible to interphase short circuits. When a fault occurs in the machine, heat is generated in the faulty winding. Due to the overlapping winding structure of the LPPPMV machine, this heat can be transferred to the healthy winding. When the healthy windings are subjected to overheating, the machine's performance degrades.

By rationally arranging the winding, this section proposes a modular asymmetric winding configuration of an LPPPMV machine. The overlapped windings are divided into three modules with an isolated winding. Fig. 11 shows the winding connection diagram of the modular LPPPMV machine. Its key structural feature is the division of the winding into three physically and electrically isolated modules. Specifically, the original three-phase winding set ABC is extended into three independent three-phase winding systems, denoted as ABC, DEF, and GHI. The original overlapping winding structure is replaced by three physically isolated three-phase winding groups, eliminating any physical contact to ensure thermal isolation. Electrical isolation is then realized by supplying each of the three sets ABC, DEF, and GHI with an independent standard inverter. Exhibiting identical MMF distribution and thrust performance to the original counterpart under healthy conditions, the modular LPPPMV machine retains all the inherent advantages of the LPPPMV topology, including high back EMF and high thrust density. Meanwhile, the LPPPMV machine with isolated winding configuration exhibits significantly improved fault-tolerant capability compared with its non-modular counterpart, enabling it to handle various fault types while ensuring normal operation.

In the modular LPPPMV machine, when an open-circuit fault occurs in one three-phase winding set, the faulty winding set can be promptly disconnected from the power supply by virtue of the modular configuration. Consequently, the remaining two healthy three-phase winding sets can continue to operate, albeit with an approximate one-third reduction in thrust output. In the event of a short-circuit fault in one three-phase winding set, the faulty set can be actively short-circuited by simultaneously turning on the upper and lower switches of the corresponding inverter legs, a method commonly referred to as active short-circuit (ASC). Owing to the inherently high self-inductance of the LPPPMV machine, this method effectively limits the steady-state short-circuit current. Owing to the modular configuration, a fault occurring in any three-phase winding set can be effectively isolated without affecting the operation of the remaining two healthy sets. These healthy winding sets continue to generate thrust based on the magnetic field modulation principle, ensuring that the fault is confined to the affected phase.

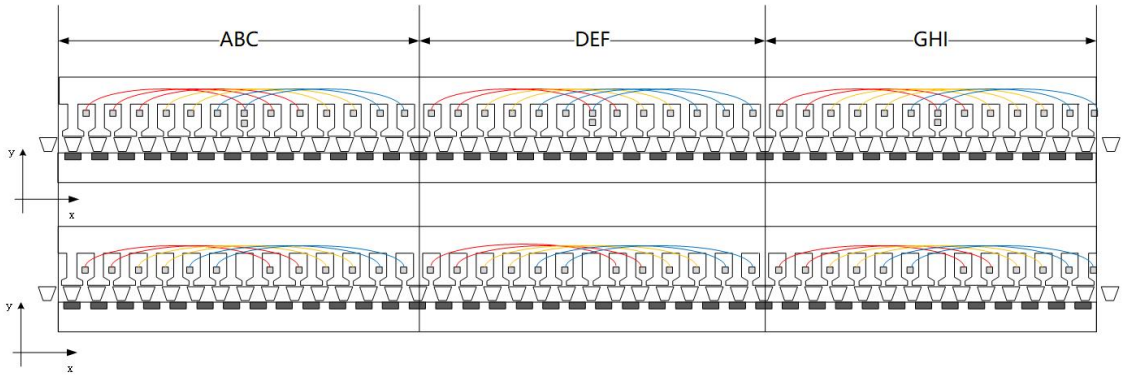

FIGURE 11. Winding configuration of the modular LPPPMV machine.

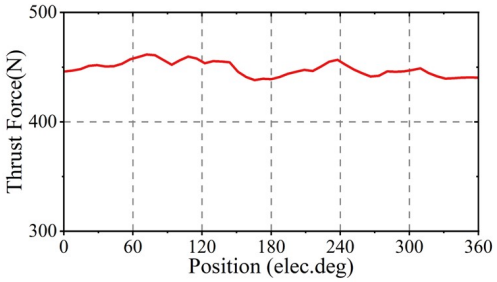

FIGURE 12. Thrust force of the modular LPPPMV machine in healthy condition.

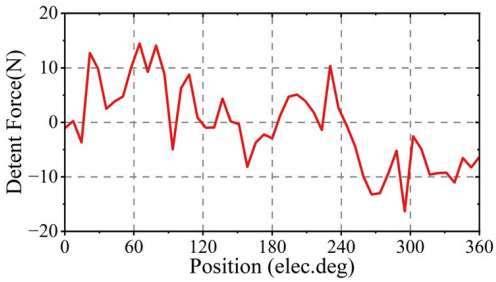

FIGURE 13. Detent force of modular LPPPMV machine.

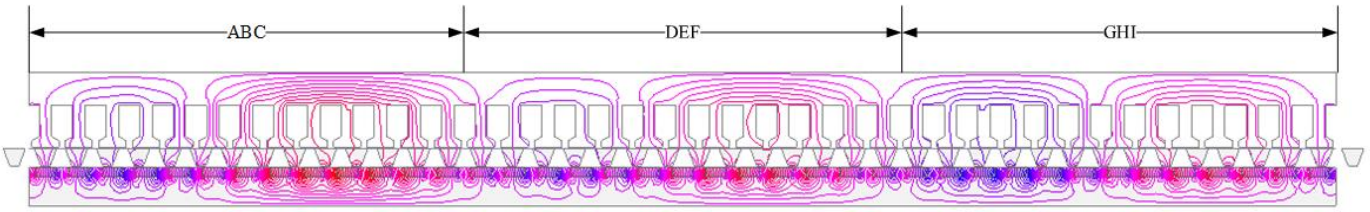

FIGURE 14. Flux distribution of modular LPPPMV machine in healthy condition.

4.2. Fault Tolerant Performance Analysis

The performance analysis of the modular LPPPMV machine is conducted under both healthy and faulty conditions. The rated current and rated speed under healthy conditions are consistent with the parameters specified in Table 1, while the fault scenarios considered involve open-circuit and short-circuit faults in the adjacent three-phase winding set. Although the machine model employed herein has been optimized, the detailed optimization process is not presented, as it is beyond the scope of this study.

Figure 12 presents the thrust force waveform of the modular LPPPMV machine under healthy operating condition. The conventional LPPPMV machine employs a single set of three-phase winding, whereas the modular LPPPMV machine utilizes three sets of three-phase winding. Except for the winding configuration, all operating parameters of the two machines are identical. Both machines were operated at their rated current of 1 A and a speed of 1 m/s. The modular LPPPMV machine produced an average thrust force of 448 N, which is comparable to that of the conventional machine.

As illustrated in Fig. 13, the detent force of the modular LPPPMV machine is significantly smaller than its average thrust force. This favorable characteristic is attributed to the reduced end-winding force and slotting force inherent to the modular design, resulting in superior overall thrust ripple performance compared with conventional linear machines.

Figure 14 shows the 2D flux distribution of the modular LPPPMV machine under healthy conditions. It can be observed from Fig. 14 that the magnetic field generated by the windings couples with that produced by the PMs, forming a triple-periodic magnetic field, which demonstrates the rationality of the machine design.

Figure 15 presents a comparative analysis of the thrust waveforms for both the modular LPPPMV machine and the conventional LPPPMV machine under healthy operating conditions and during an open-circuit fault in the ABC winding set. As observed in Fig. 15, the conventional LPPPMV machine experiences significant phase unbalance under open-circuit condition, which results in huge thrust ripple and renders the machine inoperable. This figure demonstrates that the conven-

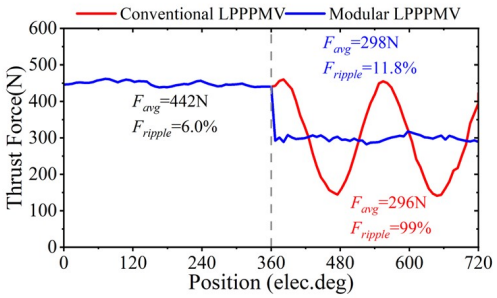

FIGURE 15. Thrust force with ABC open-circuited.

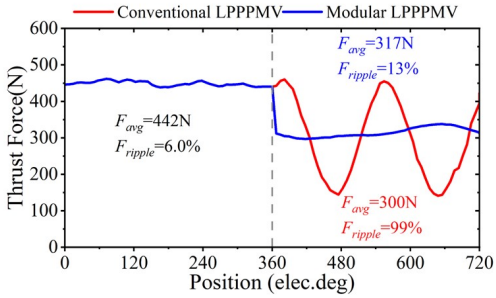

FIGURE 16. Thrust force with ABC short-circuited.

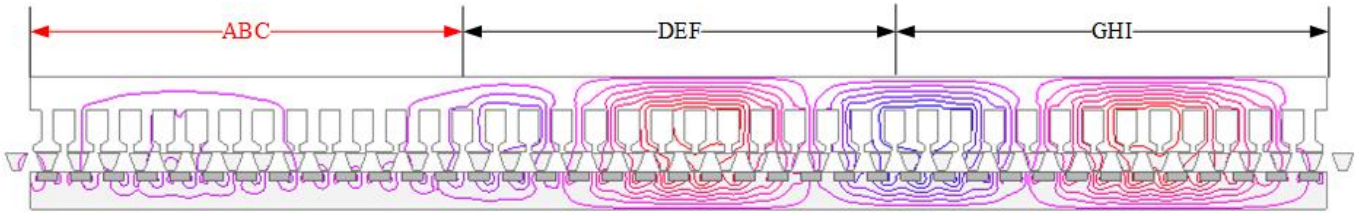

FIGURE 17. Flux distribution of modular LPPPMV machine with ABC open-circuited.

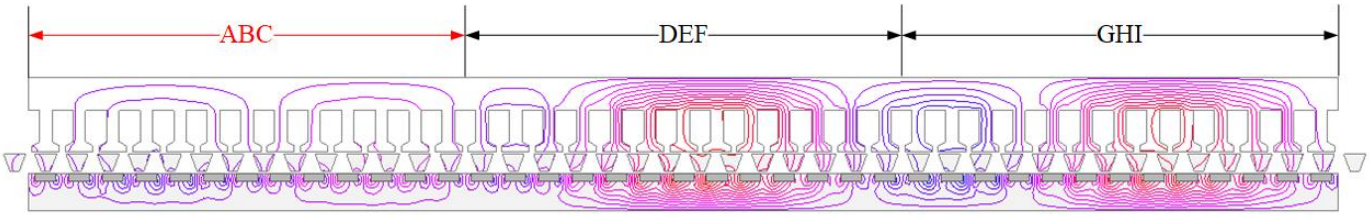

FIGURE 18. Flux distribution of modular LPPPMV machine with ABC short-circuited.

tional LPPPMV machine lacks open-circuit fault-tolerant capability. For the modular LPPPMV machine, when an open-circuit fault occurs, the current in the faulty winding will drop to zero. Benefiting from the electrical isolation between the winding sets, the remaining healthy windings can still maintain their rated current. These healthy winding sustain thrust force generation based on the principle of magnetic field modulation. The thrust force of the modular LPPPMV machine is 298 N with set ABC open circuited, basically equal to 67% of the rated value.

When a short-circuit fault occurs in one phase winding of the modular LPPPMV machine, the affected winding forms a terminal short-circuit, leading to an increase in its phase current. Benefiting from the modular design, the remaining two sets of healthy three-phase windings are electrically isolated and continue to operate under rated current conditions.

Figure 16 illustrates the thrust waveform comparison of the conventional LPPPMV machine and its modular counterpart under healthy operating conditions and during a short-circuit fault in the ABC winding set. Similar to the open-circuit condition, the modular LPPPMV machine achieves a thrust force of 317 N in the short-circuit fault-tolerant operation, which is close to two-thirds of the rated thrust force. The thrust force ripple is slightly higher than that under the open-circuit condition. This increase can be attributed to the short-circuit current in the faulty three-phase winding set, which generates a magnetic flux that interferes with the flux of the healthy three-phase winding, thereby amplifying the thrust force ripple. The above analysis verifies that the modular LPPPMV machine can accommodate three-phase winding short-circuit faults.

Figure 17 shows the modular LPPPMV machine's 2D flux distributions of phases DEF and GHI under both healthy operating conditions and during an open-circuit fault in the three-phase ABC winding set. It can be observed from the figure that the third-order harmonic in the machine is reduced while the lower-order harmonics increase. According to the magnetic field modulation theory, the third-order harmonic contributes to average thrust, whereas the lower-order harmonics tend to produce thrust force ripple. This indicates that the average thrust force decreases while the thrust force ripple increases under this condition.

Figure 18 illustrates the modular LPPPMV machine's 2D flux distribution under a three-phase short-circuit fault condition in the ABC winding set. As observed, within the machine's active region, although a short-circuit current continues to flow in the faulty ABC winding set, the flux in this region becomes unbalanced, resulting in a decrease in flux density. This reduction similarly leads to a decline in the machine's output thrust force. By contrast, the flux density distribution in the remain-

ing healthy three-phase winding set regions remains normal, allowing them to continue generating effective thrust force.

Figure 19 presents the short-circuit current waveform of the machine under a short-circuit condition in the three-phase ABC winding set. As observed, the amplitude of the short-circuit current is lower than the rated current. This attenuation is attributed to the inherently high self-inductance of the LPPPMV machine, which effectively suppresses the short-circuit current. The resultant low short-circuit current reduces the heat generated within the faulty winding set. Since the short-circuit current remains below the rated current, the heat produced by the faulty winding set does not exceed that generated under normal healthy conditions, thereby allowing the machine to maintain safe and continuous operation.

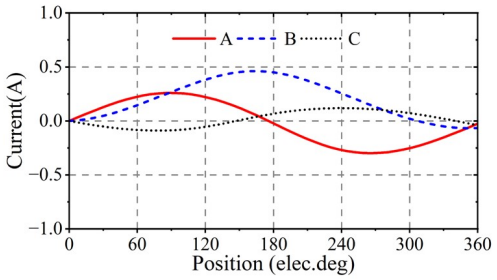

FIGURE 19. Short-circuit phase currents.

5. EXPERIMENTAL VERIFICATION

To validate the feasibility of asymmetric windings in improving the thrust-force performance of LPPPMV machines, a prototype with an asymmetric winding configuration was designed and manufactured according to the geometric parameters listed in Table 1. The rated speed is selected as 1 m/s for the test. The prototype test platforms are shown in Fig. 20. The no-load back-EMF and thrust-force performances calculated through FEM and experiments are compared and analyzed as follows.

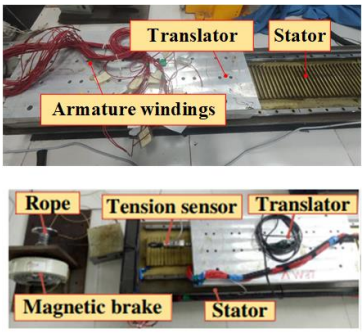

FIGURE 20. Prototype test platform of the modular LPPPMV machine.

Figure 21 depicts the set ABC's waveform of the experimental back EFM. The comparison of the A-phase no-load back EFM obtained from finite element analysis (FEA) and measurement is depicted in Fig. 22, and the comparison of its harmonic spectra is shown in Fig. 23. The measured A-phase no-load back EMF exhibits a highly sinusoidal waveform. Furthermore, it demonstrates strong agreement with the A-phase no-load back EMF obtained through FEA. It is noteworthy that

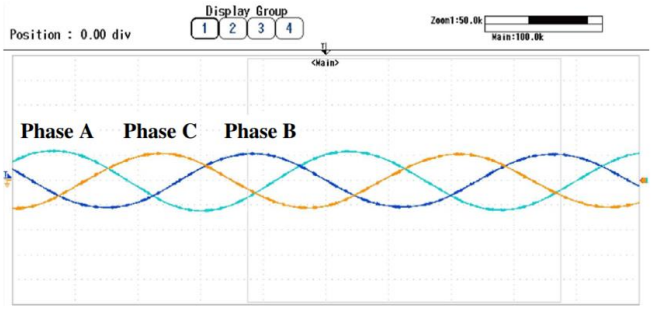

FIGURE 21. No-load back EMF of the tested prototype.

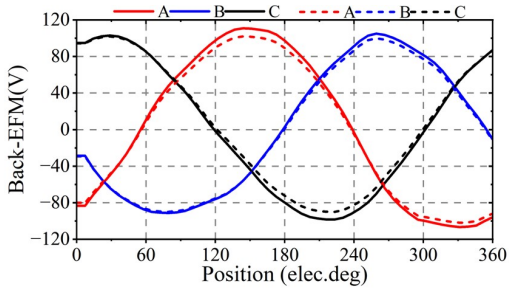

FIGURE 22. Waveform of FEM and measured back EFM.

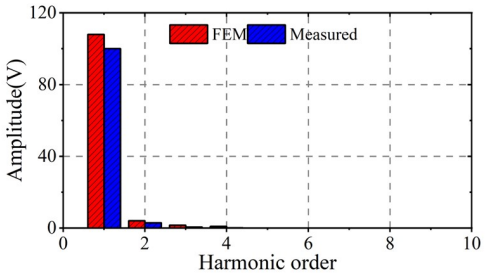

FIGURE 23. Spectrum of A-phase back EFM and measured.

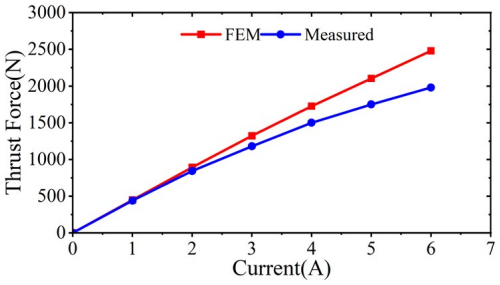

FIGURE 24. Predicted and experimental thrust force with different currents.

due to factors such as manufacturing precision of the prototype, the experimental results are approximately 6.4% lower than the simulated ones.

The comparison of thrust force obtained from experiment and FEM of the asymmetric winding configuration modular LPPPMV machine with different currents is depicted in Fig. 24. At rated current, the error of thrust force obtained from the test and FEA is approximately 1.8%. With increasing current, the error in thrust force becomes larger. This is because, as the

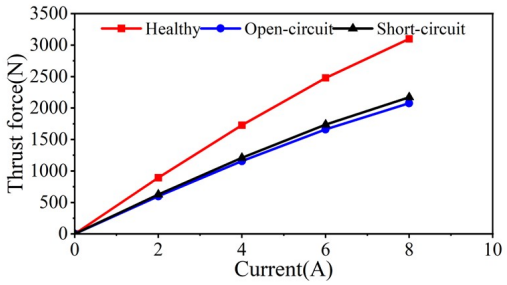

FIGURE 25. Thrust force comparison with set ABC open and short circuited.

machine runs for a longer time during the experiment, the heat generated causes magnetic saturation in the machine's magnetic circuit, thereby reducing the machine's operating efficiency.

The experimental platform also carried out experiments under open-circuit and short-circuit conditions. During the test, since the drivers are independent, the three-phase set ABC is set to open-circuit and short-circuit conditions, while the three-phase set DEF and GHI are set to a healthy condition. Fig. 25 shows the thrust of the motor under different currents in healthy, open-circuit, and short-circuit conditions. From the figure, it can be seen that under set ABC open-circuit conditions, the machine can provide 67% of the thrust force under healthy conditions, while under set ABC short-circuit conditions, it can provide 70% of the thrust force under healthy conditions, which is consistent with the previous simulation results.

6. CONCLUSION

In this article, two different armature configurations for the LPPPMV machine are designed and analyzed. The operational principle of the machine is analyzed from the perspective of MMF. The characteristics of the asymmetric winding are examined, and the back EFM and thrust of two machines are compared and evaluated. First, the topologies of the two LPPPMV machines are introduced. Then, using a complex decomposition method, the winding factor and harmonic distributions of the two types of symmetric and asymmetric winding configurations were analyzed from the perspective of winding MMF. Subsequently, the harmonic distribution in the machine's air-gap flux density was analyzed, and its relationship satisfied the magnetic-field modulation theory, explaining the working principle of the asymmetric winding. Then, a modular asymmetric winding configuration LPPPMV machine was proposed and optimized. The fault-tolerant performance of the machine was analyzed, and the problem of poor fault-tolerant performance caused by the long coil span of traditional winding was solved. Finally, a series of experiments is conducted to validate the thrust force improvement of the asymmetric winding.

ACKNOWLEDGEMENT

This work was supported in part by the National Natural Science Foundation of China under Grant 52307057 and 52207056, in part by the Natural Science Foundation of Jiangsu Province under Grant BK20230539, and in part by the Key Research and Development of Zhenjiang under Grant GY2023011.

REFERENCES

[1] Zhi, R., B. Liu, G. Lv, L. Cui, and T. Zhou, "Characteristics analysis of novel transverse flux linear synchronous motor for maglev transportation," *IEEE Transactions on Transportation Electrification*, Vol. 9, No. 3, 4104–4112, Sep. 2023.

[2] Shen, Y., Z. Li, Z. Zeng, Q. Lu, and C. H. T. Lee, "Quantitative analysis of asymmetric flux reversal permanent magnet linear machine for long excursion application," *IEEE Transactions on Industrial Electronics*, Vol. 71, No. 10, 12 781–12 792, Oct. 2024.

[3] Chen, H., Y. Meng, Q. Zhang, D. Li, and R. Qu, "Design and analysis of a new asymmetric consequent-pole flux reversal dual-pm excited machine with trapezoidal pms," *IEEE Transactions on Transportation Electrification*, Vol. 11, No. 4, 8702–8713, Aug. 2025.

[4] Ge, J., W. Xu, Y. Liu, F. Xiong, and D. Li, "Investigation on winding theory for short primary linear machines," *IEEE Transactions on Vehicular Technology*, Vol. 70, No. 8, 7400–7412, Aug. 2021.

[5] Naderi, P. and A. Shiri, "Modeling of ladder-secondary-linear induction machine using magnetic equivalent circuit," *IEEE Transactions on Vehicular Technology*, Vol. 67, No. 12, 11 411–11 419, Dec. 2018.

[6] Min, S. G., "Integrated design method of linear PM machines considering system specifications," *IEEE Transactions on Transportation Electrification*, Vol. 7, No. 2, 804–814, Jun. 2021.

[7] Cheng, M., P. Han, and W. Hua, "General airgap field modulation theory for electrical machines," *IEEE Transactions on Industrial Electronics*, Vol. 64, No. 8, 6063–6074, Aug. 2017.

[8] Du, Y., M. Cheng, K. T. Chau, X. Liu, F. Xiao, W. Zhao, K. Shi, and L. Mo, "Comparison of linear primary permanent magnet vernier machine and linear vernier hybrid machine," *IEEE Transactions on Magnetics*, Vol. 50, No. 11, 1–4, Nov. 2014.

[9] Shi, C., R. Qu, D. Li, X. Ren, Y. Gao, and Z. Chen, "Analysis of the fractional pole-pair linear PM Vernier machine for force ripple reduction," *IEEE Transactions on Industrial Electronics*, Vol. 68, No. 6, 4748–4759, Jun. 2021.

[10] Liu, G., H. Zhong, L. Xu, and W. Zhao, "Analysis and evaluation of a linear primary permanent magnet vernier machine with multiharmonics," *IEEE Transactions on Industrial Electronics*, Vol. 68, No. 3, 1982–1993, Mar. 2021.

[11] Du, K., W. Zhao, L. Xu, and J. Ji, "Design of a new fault-tolerant linear permanent-magnet vernier machine," *IEEE Journal of Emerging and Selected Topics in Industrial Electronics*, Vol. 1, No. 2, 172–181, Oct. 2020.

[12] Zhao, W., S. Wang, J. Ji, L. Xu, and Z. Ling, "A new mover separated linear magnetic-field modulated motor for long stroke applications," *IEEE Transactions on Magnetics*, Vol. 53, No. 11, 1–5, Nov. 2017.

[13] Lu, Q., B. Wu, Z. Zeng, and X. Huang, "Analysis of a new partitioned-primary flux-reversal hybrid-excited linear motor," *IEEE Transactions on Industry Applications*, Vol. 57, No. 1, 448–457, Jan.-Feb. 2021.

[14] Zeng, Z., Y. Shen, Q. Lu, B. Wu, D. Gerada, and C. Gerada, "Investigation of a partitioned-primary hybrid-excited flux-switching linear machine with dual-PM," *IEEE Transactions on Industry Applications*, Vol. 55, No. 4, 3649–3659, Jul.-Aug. 2019.

[15] Xu, Y., J. Ji, Z. Ling, C. Wang, and W. Zhao, "Quantitative comparison of modular linear permanent magnet vernier machines with and without partitioned primary," *Chinese Journal of Electrical Engineering*, Vol. 9, No. 3, 72–83, Sep. 2023.

[16] Cheng, M., W. Qin, X. Zhu, and Z. Wang, "Magnetic-inductance: Concept, definition, and applications," *IEEE Transactions on Power Electronics*, Vol. 37, No. 10, 12 406–12 414, Oct. 2022.

[17] Metwly, M. Y., M. Ahmed, A. Hemeida, A. S. Abdel-Khalik, M. S. Hamad, A. Belahcen, S. Ahmed, and N. A. Elmalhy, "Investigation of six-phase surface permanent magnet machine with typical slot/pole combinations for integrated onboard chargers through methodical design optimization," *IEEE Transactions on Transportation Electrification*, Vol. 9, No. 1, 866–885, 2022.

[18] Han, S.-H., T. M. Jahns, W. L. Soong, M. K. Güven, and M. S. Illindala, "Torque ripple reduction in interior permanent magnet synchronous machines using stators with odd number of slots per pole pair," *IEEE Transactions on Energy Conversion*, Vol. 25, No. 1, 118–127, Mar. 2010.

[19] Li, J., Y. Xu, J. Zou, B. Wang, Q. Wang, and W. Liang, "Analysis and design of spm machines with fractional slot concentrated windings for a given constant power region," *IEEE Transactions on Magnetics*, Vol. 51, No. 11, 1–4, Nov. 2015.

[20] Yan, D., Z. Zhu, H. Lei, Y. Yan, T. Shi, and C. Xia, "Investigation of asymmetrical winding layouts for fractional-slot permanent magnet machine," *IEEE Transactions on Industrial Electronics*, Vol. 71, No. 8, 8416–8426, Aug. 2024.

[21] Demir, Y., A. M. El-Refaie, and M. Aydin, "Investigation of asymmetric and unbalanced winding structures for 3-phase permanent magnet synchronous machines," *IEEE Transactions on Energy Conversion*, Vol. 36, No. 3, 1722–1732, Sep. 2021.

[22] Demir, Y. and M. Aydin, "Design of several un-skewed radial flux permanent magnet synchronous motors with asymmetric and symmetric AC windings — A comparative study," in *2014 IEEE Energy Conversion Congress and Exposition (ECCE)*, 2411–2417, Pittsburgh, PA, USA, 2014.